Geophysical Research Letters

RESEARCH LETTER
10.1029/2022GL100654

Key Points:

- Convective instabilities may govern vertical ice front melting at low ambient currents but are ignored in existing parameterizations
- We propose a novel melt parameterization for vertical fronts continuous across convective and shear regimes constrained by observations
- The contribution of background melting as opposed to melting within subglacial discharge plumes might be larger than previously thought

Correspondence to:
K. Schulz,
kiki.schulz@utexas.edu

Citation:
Schulz, K., Nguyen, A. T., & Pillar, H. R. (2022). An improved and observationally-constrained melt rate parameterization for vertical ice fronts of marine terminating glaciers. *Geophysical Research Letters*, *49*, e2022GL100654. https://doi.org/10.1029/2022GL100654

Received 30 JUL 2022
Accepted 19 SEP 2022

An Improved and Observationally-Constrained Melt Rate Parameterization for Vertical Ice Fronts of Marine Terminating Glaciers

K. Schulz[1], A. T. Nguyen[1], and H. R. Pillar[1]

[1]Oden Institute for Computational Engineering and Sciences, The University of Texas at Austin, Austin, TX, USA

Abstract Submarine melting at Greenland's marine terminating glaciers is a crucial, yet poorly constrained process in the coupled ice-ocean system. Application of Antarctic melt rate representations, derived for floating glacier tongues, to non-floating marine terminating glaciers commonly found in Greenland, results in a dramatic underestimation of submarine melting. Here, we revisit the physical theory underlying melt rate parameterizations and leverage recently published observational data to derive a novel melt rate parameterization. This is the first parameterization that (a) consistently comprises both convective- and shear-dominated melt regimes, (b) includes coefficients quantitatively constrained using observational data, and (c) is applicable to any vertical glacier front. We show that, compared to the current state-of-the-art approach, the scheme provides an improved fit to observed melt rates on the scale of the terminating front, offering an opportunity to incorporate this critical missing forcing into ocean circulation models.

Plain Language Summary Where Greenland's glaciers terminate in the ocean, the relatively warm waters in the fjords melt the ice. This is a very important process, as the rate of melt determines how fast the glaciers are losing mass and inject freshwater into the ocean, which contributes to sea level rise and can change ocean currents. Unfortunately, it is still difficult to calculate how much glacial ice is melted by the warm ocean around Greenland, as it is unfeasible to measure the small melting processes so close to the calving glacier front. Up to now, melt rate calculations rely on estimates for floating glacier tongues in Antarctica, which are more accessible, but it has become increasingly apparent that important differences exist for these two cases. In this study, we try to find a better way to calculate melt rates for marine terminating glaciers with vertical fronts, by reconsidering the underlying physics of submarine melt, and by using observations of submarine melt waters near a vertical glacier front in Alaska.

1. Introduction

Submarine melting of Greenland's marine terminating glaciers accounts for a substantial mass loss of the Greenland Ice Sheet, accelerating with warming of subpolar North Atlantic waters (Cowton et al., 2018; Fahrner et al., 2021; Straneo & Heimbach, 2013). Melting by deep, warm waters increases undercutting of glacier termini, thereby inducing calving (Wood et al., 2021) and glacier front retreat (King et al., 2020), leading to a dynamic mass loss that adds to sea level rise (Mouginot et al., 2019). Freshwater input resulting from submarine melt controls the stratification and buoyancy driven circulation within Greenland's fjords (Straneo et al., 2011), and affects the adjacent shelf sea (Huhn et al., 2021; Le Bras et al., 2018) and global scale ocean circulation patterns (Bakker et al., 2016; Böning et al., 2016; Frajka-Williams et al., 2016; Thornalley et al., 2018; Yang et al., 2016). Given the important role of submarine melting, a precise constraint of the ice-ocean interaction at marine terminating vertical glacier fronts is crucial to derive melt parameterizations for ocean circulation models (Straneo & Cenedese, 2015). However, as calving fronts are a highly dangerous environment, few observations are available. As a result, observations obtained from more accessible Antarctic floating glacier tongues have been used to derive a melt rate parameterization that is commonly also applied to calculate submarine melt at non-floating glacier termini (Malyarenko et al., 2020, and the references therein). Recent studies suggest, however, that this parameterization dramatically underestimates submarine melt rates at vertical ice fronts (Jackson et al., 2020; Sutherland et al., 2019a).

In this study, we revisit the standard melt parameterization from Jenkins et al. (2010) to reconsider its applicability to vertical glacier fronts. We propose an alternative formulation accounting for convective instabilities which have been found to control dynamics near the ice-ocean interface in low-shear regimes (Section 2). We run an

ensemble of meltwater plume simulations, that is, buoyant plumes induced by submarine melting (Section 3), and determine an associated thermal transfer velocity, γ_T, providing the optimal fit to recent and unique observations (Jackson et al., 2020) of melt water intrusions at a vertical ice front (Section 4.1). In Section 4.2, we extend our parameterization to allow for augmented thermal transfer through the transition to high-velocity (shear-driven) melt regimes. This melt rate parameterization is evaluated against observational melt rate estimates from marine terminating glaciers in Greenland and Alaska (Section 4.3).

2. Theoretical Background

At the interface of ice with a temperature T_i (commonly −10°C) and zero salinity, and the ocean at temperature T and salinity S, submarine melting is described by solving

$$\dot{m}\left(c_i\left(T_b - T_i\right) + L\right) = \gamma_T c_w \left(T - T_b\right) \tag{1}$$

$$\dot{m} S_b = \gamma_S \left(S - S_b\right) \tag{2}$$

$$T_b = \lambda_1 S_b + \lambda_2 + \lambda_3 z \tag{3}$$

for the melt rate $\dot{m}$, and the temperature and salinity at the ice-ocean boundary T_b and S_b (e.g., Malyarenko et al., 2020). The specific heat capacities of ice $c_i = 2000$ J kg^{-1} C^{-1} and water $c_w = 3974$ J kg^{-1} C^{-1} are well constrained, along with the latent heat of melting ice $L = 3.35 \times 10^5$ J kg^{-1} in Equation 1, and the empirical constants $\lambda_1 = -5.73 \times 10^{-2}$°C psu^{-1}, $\lambda_2 = 8.32 \times 10^{-2}$ °C, and $\lambda_3 = 7.61 \times 10^{-4}$ °C m^{-1} in Equation 3. In contrast, the optimal choice of γ_T and γ_S is less straightforward.

The parameters $\gamma_{T,S}$ can be interpreted as characteristic velocities for the transfer of heat and salt across infinitesimal sublayers. Assuming a frictional boundary layer controlled by shear instabilities at the ice-ocean interface, as proposed for sea ice (McPhee et al., 1987) and quasi-horizontal floating ice shelves in Antarctica (Scheduikat & Olbers, 1990), the transfer velocities γ_T and γ_S scale with the respective molecular diffusivities $\kappa_{T,S}$, and the thickness of the thermal and haline viscous sublayer, which in turn depend on the ambient friction velocity. Based on these theoretical considerations and observed melt rates of Antarctic ice shelves, past studies have chosen the transfer velocities $\gamma_{T,S}$ to be constant, implicitly assuming a representative friction velocity (e.g., Hellmer & Olbers, 1989; Scheduikat & Olbers, 1990), or to be a function of the (variable) ambient velocity, typically the velocity of the adjacent subglacial discharge plume or a tidal or mean current, u,

$$\gamma_{T,S} = \Gamma_{T,S} C_d^{0.5} u, \tag{4}$$

where C_d is a dimensionless drag coefficient and $\Gamma_{T,S}$ are dimensionless turbulent transfer coefficients for heat and salt (e.g., Holland & Jenkins, 1999; Jenkins, 1991). This functional form, with parameters $\Gamma_{T,S}$ and C_d constrained using data from the Ronne Ice Shelf (Jenkins et al., 2010), is commonly applied in fjord-scale models (e.g., Beckmann et al., 2018; Cowton et al., 2015; Jackson et al., 2017; Sciascia et al., 2013; Xu et al., 2013).

The applicability of the Jenkins et al. (2010) melt rate parameterization to the vertical fronts of Greenland's glaciers is, however, questionable. The lack of observational data has so far prevented a quantitative verification of the parameterization for vertical ice fronts, and restricted advances in this field to modeling studies. Besides the lack of a quantitative constraint of the transfer velocities, a major concern regarding the standard parameterization is the unrealistic disappearance of submarine melting with diminishing ambient water velocities, as implied by the proportionality of $\gamma_{T,S}$ and u (Equation 4). In recent efforts, this effect was mitigated by introducing a minimum, or background, velocity u_t to the standard parameterization (e.g., Cowton et al., 2015; Slater et al., 2015). While this modification mitigates the issue of vanishing background melt, it is not based on physical theory and introduces another unconstrained parameter, u_t, on which simulations are sensitively dependent (Cowton et al., 2015).

In a laboratory experiment, McConnochie and Kerr (2017) tested the validity of Equation 4 from Jenkins et al. (2010) near vertical interfaces, and found this functional dependence to only hold in the presence of ambient velocities u greater than a threshold of approximately 0.04 m s^{-1}. Below this threshold, transfer velocities were found to be constant. This transition is attributed to a regime change from a laminar sublayer controlled by convective instabilities at low fluid velocities, to a sublayer controlled by shear instabilities at greater fluid velocities. These findings encourage a melt rate parameterization incorporating constant $\gamma_{T,S}$ at sub-threshold

velocities and velocity-dependent $\gamma_{T,S}$ at higher ambient velocities, thus providing a physical meaning to the background velocity u_r. Laboratory experiments have also provided an updated assessment of the correct proportionality between γ_T and γ_S. The ratio corresponding to the standard transfer velocities proposed by Jenkins et al. (2010) was found to be too small by a factor of 2.6 (Kerr & McConnochie, 2015). Based on theoretical considerations of the relative thickness of the thermal and haline sublayer and experimental results, Kerr and McConnochie (2015) found

$$\frac{\gamma_S}{\gamma_T} = \left(\frac{\kappa_S}{\kappa_T}\right)^{0.5} \approx 0.07 \tag{5}$$

for water temperatures up to 6°C.

Independently, both high-resolution, non-hydrostatic modeling studies (Sciascia et al., 2013) and observational data (Jackson et al., 2020) suggest that melting at vertical glacier fronts, in the absence of subglacial discharge, creates buoyant plumes that rise parallel to the ice-ocean interface until they reach neutral buoyancy. We will refer to plumes induced by submarine melting as "meltwater plumes," in contrast to "subglacial discharge plumes." The velocity of these meltwater plumes is found to be ∼0.04 m s^{-1} (vertical velocity, Sciascia et al., 2013) and 0.034 m s^{-1} (horizontal velocity anomaly of meltwater intrusions away from the glacier front, Jackson et al., 2020). These values are close to the threshold velocity for the regime transition found in idealized laboratory settings by McConnochie and Kerr (2017), and indicate that both convective and shear-driven instabilities are relevant for ice-ocean exchange at these vertical glacier fronts.

For boundary layers controlled by convective instabilities, the evolution of a meltwater plume with width b, vertical velocity u_p, temperature T_p, and salinity S_p along the vertical coordinate z can be described by the following four equations conserving mass, momentum, heat and salt (following Wells & Worster, 2008):

$$\frac{d}{dz}(bu_p) = E_0 u_p + \dot{m} \tag{6}$$

$$\frac{d}{dz}\left(bu_p^2\right) = bg\Delta\rho \tag{7}$$

$$\frac{d}{dz}(bu_pT_p) = E_0 u_p T_a + \dot{m}T_b - \gamma_T(T_p - T_b) \tag{8}$$

$$\frac{d}{dz}(bu_pS_p) = E_0 u_p S_a + \dot{m}S_b - \gamma_S(S_p - S_b)\,, \tag{9}$$

where $E_0 = 0.1$ is the entrainment parameter, $g = 9.81$ m s^{-1} is the gravitational acceleration, $\Delta\rho = \frac{\rho_a - \rho}{\rho_0}$ is the density deficit of the plume with $\rho_0 = 1{,}024$ kg m^{-3}, and T_a and S_a are the ambient water temperature and salinity, respectively. The transfer velocities $\gamma_{T,S}$ in Equations 8 and 9 are assumed to be constant and independent of the plume velocity u_p. In contrast to commonly used models for subglacial discharge plumes (e.g., Cowton et al., 2015; Beckmann et al., 2018; Hewitt, 2020, and the references therein), which are characterized by higher plume velocities and are hence controlled by shear instabilities, Equations 6–9 do not include frictional effects and are therefore independent of the choice of a drag coefficient. Under the assumption of a frictional boundary layer, associated with higher plume velocities, Equation 7 includes an additional term $-C_d u_p^2$, and the transfer velocities $\gamma_{T,S}$ in Equations 8 and 9 follow Equation 4 with $u = u_p$ (see e.g., Jackson et al., 2020; Jenkins, 2011).

Recent observations of meltwater intrusions near LeConte glacier, acquired away from the influence of subglacial discharge, allows melt rate parameters for vertical glacier fronts to be quantitatively constrained for the first time (Jackson et al., 2020). Under the assumption of rising meltwater plumes governed by frictional effects associated with shear instabilities, Jackson et al. (2020) conducted parameter studies with four free parameters, $\Gamma_{T,S}$, C_d, and the background or minimum velocity u_t (v_{hor} in Jackson et al., 2020), and compared the results of simulations against observed properties of the meltwater intrusions. The authors found that simulations using typical parameter values from Jenkins et al. (2010) underestimate observed melt rates by two orders of magnitude. Due to the large number of free parameters, however, no conclusive scaling of individual values ($\Gamma_{T,S}$, C_d, u_t) could be proposed, preventing the development of a flexible parameterization for use in ocean circulation models.

Here, we repeat the analysis from Jackson et al. (2020), but assume that the ice-ocean exchange in meltwater plumes is controlled by convective instabilities (Equations 1–3, 6–9, constant $\gamma_{T,S}$), rather than by frictional

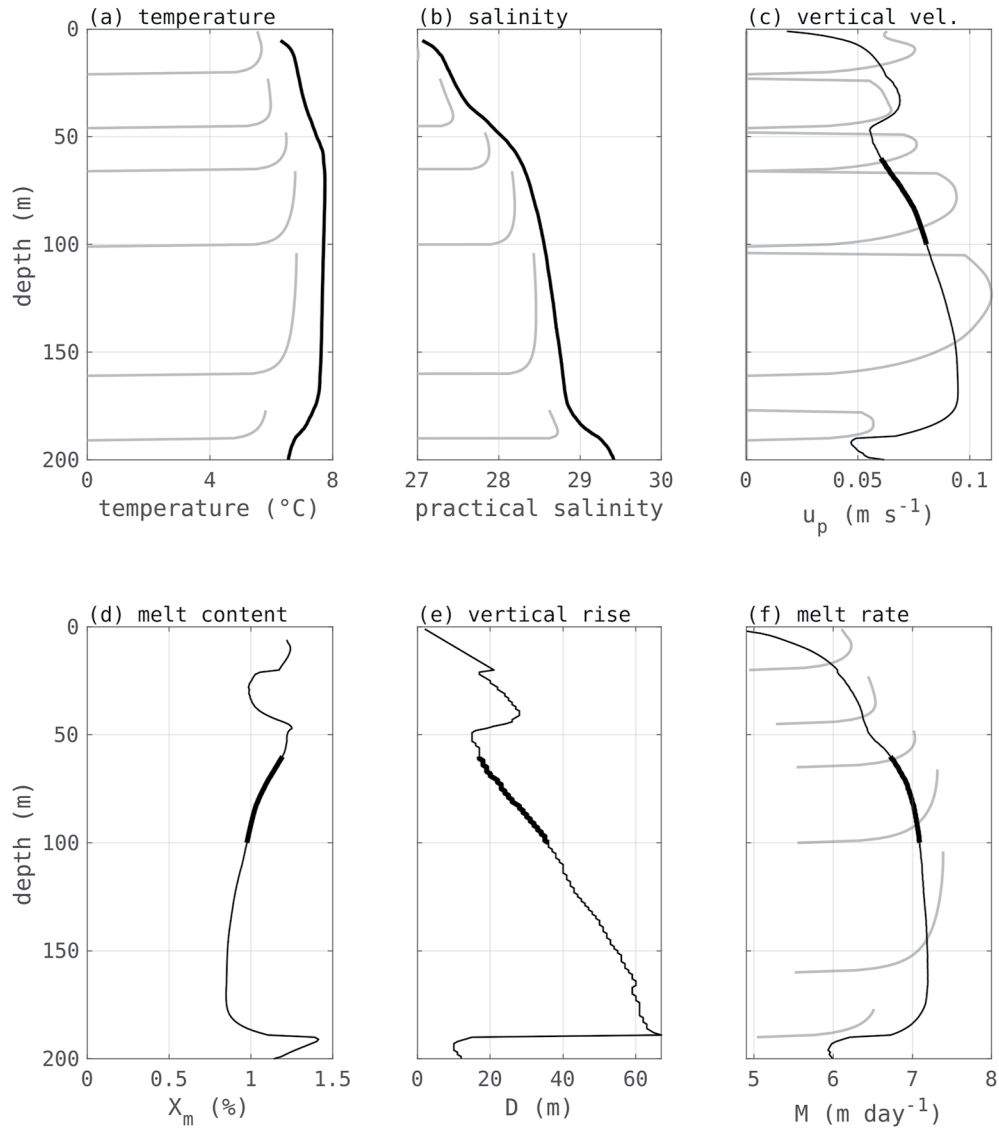

Figure 1. Black lines show the vertical distribution of observed fjord (a) temperature (°C) and (b) salinity near LeConte glacier. Black lines in (c–f) show average plume properties of the 200 member ensemble with $\gamma_T = 10^{-3}$ m s^{-1}: (c) vertical velocity (m s^{-1}), (d) melt content (%), (e) vertical rise (m), and (f) melt rate (m day^{-1}), defined relative to the initialization depth of the plume. Gray lines in (a–c and f) show properties of six example individual plumes. Thick black lines in (c–f) indicate the depth interval used for averaging simulated plumes for comparison to observations from Jackson et al. (2020) in Figure 2.

effects. This effort is motivated by the proximity of the meltwater plume velocities (Jackson et al., 2020; Sciascia et al., 2013) to the threshold velocity u_t (McConnochie & Kerr, 2017) and the highly desirable reduction in degrees of freedom achieved for a buoyancy-driven scheme. With the additional assumption of a constant proportionality between γ_T and γ_S (Equation 5), the problem is reduced to solving for only one unconstrained parameter, the thermal transfer velocity γ_T, avoiding the under-determined problem tackled by Jackson et al. (2020).

3. Methods

Following Jackson et al. (2020), we use ambient temperature and salinity profiles obtained in front of LeConte glacier in Alaska in September 2018 (black lines Figures 1a and 1b, Section 4.1) to simulate meltwater plumes, that is, plumes created by submarine melting, and examine plume property changes with variation of our one free parameter γ_T. Individual plumes were independently initialized with a freshwater flux perturbation of

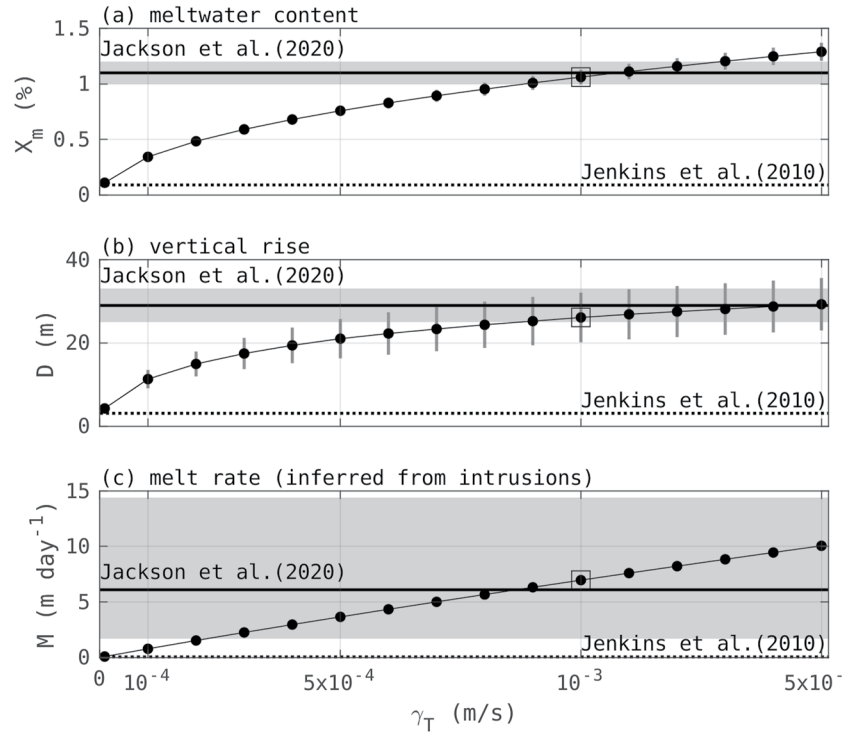

Figure 2. Comparison of observed and simulated meltwater plume properties: (a) meltwater content (%), (b) vertical rise (m), and (c) melt rate (m day^{-1}). Observed properties (horizontal black line, shading indicates bootstrap 95% confidence interval in (a and b) and range of individual estimates in (c)) are for meltwater intrusions documented by Jackson et al. (2020). Simulated properties (black dots, vertical gray lines indicate standard deviation) are for the numerical ensemble described in Section 4.1 with variable γ_T; black squares indicate the optimal value, γ_T^*, fitting the observations. Properties estimated using the standard parameterization and values from Jenkins et al. (2010) (calculated in Jackson et al. (2020)) are shown by the dotted line.

$Q = 10^{-10}$ m^2 s^{-1} at 1 m vertical spacing, and Equations 1–3, 5–9 were solved numerically (1 m resolution). Our code is adapted from the plume model developed by Cowton et al. (2015) and employs the same ODE solver.

From these numerical simulations, we calculated for each meltwater plume the vertical rise D (distance between the initialized and neutral buoyancy depth), the mean submarine melt rate M, and the average meltwater content X_m defined as

$$X_m = \frac{T_a - T_p^t}{T_a - T_m}, \tag{10}$$

where T_a is the ambient temperature, averaged over the depth range covered by the plume, T_p^t is the terminal plume temperature and $T_m = -90$°C is the effective temperature of submarine meltwater (Gade, 1979; Jackson et al., 2020). The properties of individual meltwater plumes were averaged for plumes initiated between a water depth of 60–100 m, as most melt water intrusions in Jackson et al. (2020) were observed between 30 and 70 m water depth, and the average observed vertical rise of plumes is approximately 30 m. By comparing our results (Figures 1 and 2) to the corresponding values derived from observed meltwater intrusions of $D = 29 \pm 4$ m, $X_m = 1.1 \pm 0.1\%$, and $M = 1.7$–14.4 m day^{-1} averaging 6.1 m day^{-1} from Jackson et al. (2020), we can constrain an optimal value for γ_T to reproduce these observations.

4. Results and Discussion

4.1. Deriving γ_T at Low Ambient Velocities

Simulations were run with γ_T ranging from 10^{-5} to 5×10^{-3} m s^{-1}. For $\gamma_T = 10^{-3}$ m s^{-1}, properties of the simulated meltwater plumes (i.e., plumes induced by submarine melting) are shown in Figure 1. The balance of glacial melting and the entrainment of ambient water creates meltwater plumes with a nearly constant final

temperature anomaly of ~1°C (difference between the gray and black lines in Figure 1a). The plume-averaged vertical velocities are small, less than 0.1 m s^{-1}, and on average 0.07 m s^{-1} for plumes initialized at 60–100 m water depth (Figure 1c), well in line with measured vertical velocities of melt-driven convection at iceberg fronts (0.07 m s^{-1}, Josberger & Neshyba, 1980). In the depth region of 50–170 m, where ambient temperature and salinity (Figures 1a and 1b) are relatively constant, the vertical extent of individual plumes is governed primarily by pressure effects, and the vertical rise of the plume linearly increases with initialization depth (Figure 1e). Both the melt water content and the calculated melt rates exhibit little variability in the vertical in this range (Figures 1d and 1f).

Figure 2 shows depth-averaged (60–100 m) meltwater content, vertical rise, and melt rate simulated for a range of γ_T. As stated in Jackson et al. (2020), the melt rate parameterization for floating glacier tongues in Antarctica proposed by Jenkins et al. (2010) (dotted lines, Figure 2) fails to reproduce the melt dynamics at non-floating (i.e., vertical front) marine terminating glaciers. In the theoretical framework considered here, the optimal thermal transfer velocity γ_T^*, defined as providing the best fit to the observed properties of meltwater intrusions, is $\sim 10^{-3} \pm 10^{-4}$ m s^{-1} (Figure 2). A value of γ_T that results in plume properties close to those simulated with the Jenkins et al. (2010) parameterization (Jackson et al., 2020) is two orders of magnitude smaller (Figure 2).

This γ_T^* approximately corresponds to the product $\Gamma_T C_d^{0.5} v_{hor}$ in Jackson et al. (2020), for the case where a constant background velocity, $v_{hor} = 0.2$ m s^{-1}, specific to the environment at LeConte glacier, is applied. Depending on which of these three individual parameters were modified, a value of $\Gamma_T C_d^{0.5} v_{hor} = 0.8 - 0.9 \times 10^{-3}$ m s^{-1} was found to best reproduce the observations. However, in contrast to Jackson et al. (2020), the parameterization derived here is based on the assumption of a boundary layer controlled by convective instabilities, not shear instabilities, yielding a different functional form of the parameterization independent of the ambient velocity. Hence, C_d and v_{hor} (or equivalently u_t) do not appear in the governing equations. The validity of assuming a convective–instability controlled boundary layer at low velocities is supported by previous laboratory findings (see Section 2). Applicability in the energetic environment around LeConte glacier is tested in Section 5.

4.2. Extension to Higher Ambient Velocities

Up to this point, we derived γ_T^* in a regime controlled by convective instabilities, independent of the low ambient velocity u. The question remains as to how γ_T behaves with stronger tangential currents, for example, within a subglacial discharge plume or in the presence of energetic fjord circulations. Literature results point to a threshold velocity u_t in the range of 0.03–0.07 m s^{-1}, above which a shear-driven melt parameterization should be applied. In the absence of additional observational constraints, we now explore theoretical considerations for producing a melt rate parameterization continuous across buoyancy and shear-driven regimes.

The classical Jenkins et al. (2010) parameterization (Equation 4, dashed line in Figure 3), provides the best available estimate of melt rate above the threshold velocity. Although being derived for horizontal ice-ocean interfaces, there is no obvious dependence on interface orientation, only on the existence of a shear-dominated melt regime. We therefore proceed by seeking a continuous scheme that is informed by Jenkins et al. (2010) above the threshold u_t, with our constant constrained melt rate applied below u_t. A potential approach is to enforce the zero intercept of Jenkins et al. (2010), such that the melt rate scales with $u u_t^{-1}$ above the threshold velocity. With the results derived here, this approach yields $\gamma_T = \gamma_T^* = 10^{-3}$ m s^{-1} for $u \leq u_t$ (black lines in Figure 3) and $\gamma_T = \gamma_T^* u_t^{-1} u$ at $u \geq u_t$ (gray lines in Figure 3). This approach yields some highly undesirable behavior, including a high sensitivity to the exact choice of the uncertain parameter u_t, as well as very large γ_T at high u that may be unrealistic.

A more sensible parameterization is to retain the slope proposed by Jenkins et al. (2010), giving a linear dependence of γ_T on the velocity u in a boundary layer controlled by shear instabilities, while allowing for γ_T^* at $u \leq u_t$ (orange and black lines in Figure 3). In contrast to any previously proposed melt rate parameterizations, this functional form allows for a smooth transition of γ_T about u_t and a clear interpretation of the scheme as a linear superposition of the (velocity–dependent) contribution of shear instabilities and the (constant) contribution of convective instabilities in controlling the ice–ocean boundary layer. An attractive characteristic of this parameterization is that it is weakly sensitive to the exact choice of u_t.

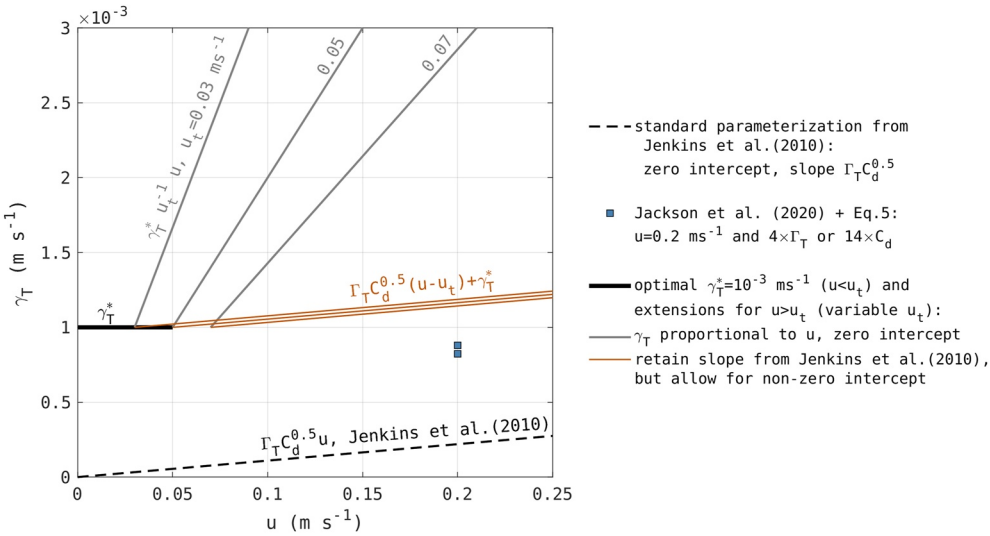

Figure 3. Possible parameterizations of the thermal transfer velocity γ_T, for threshold velocities of $u_t = 0.03, 0.05, 0.07$ m s^{-1}, in comparison to the standard parameterization proposed by Jenkins et al. (2010) (dashed black line). Blue squares show melt rate estimates provided only for LeConte by Jackson et al. (2020).

In summary, we propose a subgrid scale parameterization of the thermal transfer velocity γ_T, to describe submarine melting at the vertical glacier fronts, as follows:

$$\gamma_T = \begin{cases} \gamma_T^* & u \le u_t \\ \Gamma_T C_d^{0.5} (u - u_t) + \gamma_T^* & u \ge u_t, \end{cases} \tag{11}$$

with $\Gamma_T \sim 2.2 \times 10^{-2}$ and $C_d \sim 2.5 \times 10^{-3}$ from Jenkins et al. (2010), $u_t \sim 0.05$ m s^{-1}, and $\gamma_T^* \sim 1 \times 10^{-3}$. This parameterization includes the constant thermal transfer velocity at low ambient velocities derived in Section 4.1, and a linear superposition of this constant and a contribution proportional to u at higher ambient velocities. The optimal values of Γ_T, C_d, γ_T^*, and u_t for vertical ice fronts can be better constrained when additional relevant observations are obtained and improved numerical simulations are carried out.

4.3. Application to Non-Floating Marine Terminating Glaciers

In this section, we apply our proposed parameterization across the full width of glacier fronts, and assess its performance using existing observational estimates of submarine melt rates for marine terminating glaciers. Following Jackson et al. (2017), we simulate the evolution of subglacial discharge as truncated line plumes of width L_p with frictional boundary layers (Equations 1–3, 5–9, including the additional drag term in Equation 7), but with the functional form and values of γ_T proposed above (Equation 11). Outside of the subglacial discharge plume, we calculate melt rates within stacked meltwater plumes, as in Section 4.1 (blue lines, Figure 4). Since glacier fronts span several 100 m in the vertical, a large ensemble of plumes is required. Depending on the assumed spatial distribution of the meltwater plumes, this can be computationally expensive. To avoid the need for these large ensembles in ocean circulation models, we test the approximation of melt rates only thermodynamically, that is, directly using fjord temperature and salinity profiles in Equations 1–3, 5 (black lines, Figure 4). This simplification neglects how ambient temperature and salinity are modified within the meltwater plumes (see Figures 1a and 1b), and assumes $u < u_t$. We run simulations with γ_T^* ranging from 10^{-4}–10^{-3} m s^{-1} (Figure 4). Observational melt rate estimates and input parameters for the simulations (fjord stratification, approximate values for glacier front width and depth, width of line plume L_p and subglacial discharge Q_{sg}) are available for LeConte glacier (Jackson et al., 2020), Helheim glacier (Cowton et al., 2015; Sciascia et al., 2013; Straneo et al., 2011; Sutherland & Straneo, 2012), and Store glacier (Xu et al., 2013), as summarized in Figure 4.

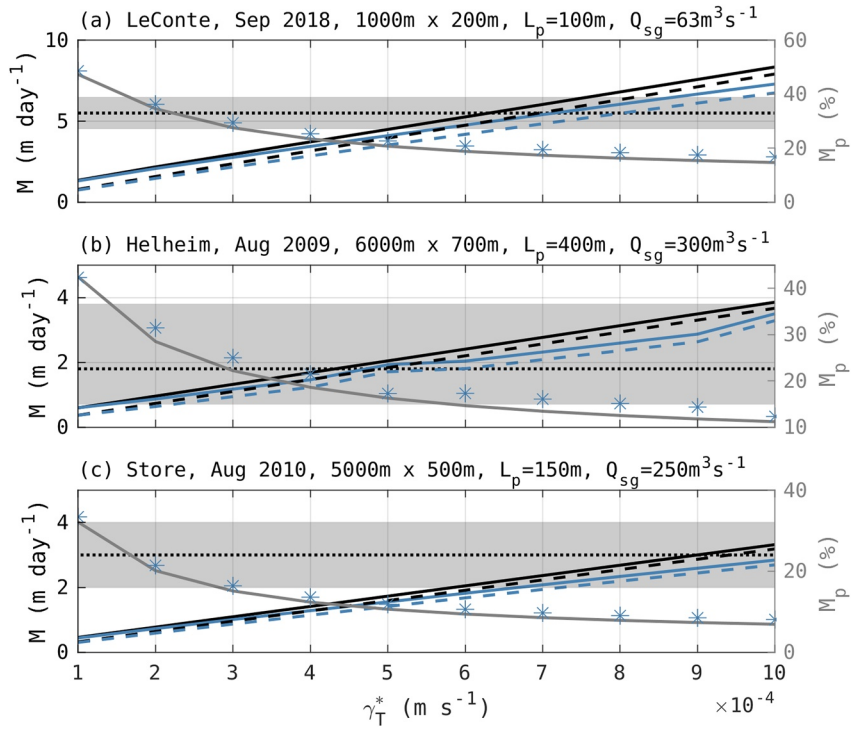

Figure 4. Left axis (m day^{-1}): Comparison between observed (dotted black line, gray shading represents the uncertainty (Jackson et al., 2020; Sutherland & Straneo, 2012; Xu et al., 2013, respectively)) and simulated terminus-averaged melt rates (solid lines). Dashed lines indicate background (i.e., outside of the subglacial discharge plume) melt rates. We compare background melt rates (blue dashed) rigorously calculated with large meltwater plume ensembles to (black dashed) an approximate calculation substituting meltwater plume temperature and salinity for ambient profiles in Equations 1–3, 5. Right axis (gray lines and blue stars, %): Relative contribution of melting within the subglacial discharge plume for (a) LeConte glacier, (b) Helheim glacier, and (c) Store glacier.

While it is technically possible to identify an optimal value of γ_T to reproduce observational estimates of melt rates, these results should be treated with great care, as most observed melt rate estimates are derived based on the instantaneous heat transport toward the glacier. These estimates are subject to large uncertainties that cannot be accurately quantified, associated with the resolution and timing of the observations, as well as iceberg melt and heat accumulation in the fjord (Jackson & Straneo, 2016).

Jackson et al. (2020) estimated the terminus-averaged melt rate for LeConte glacier to be 5.5 ± 1.0 m day^{-1}. In our simulations, good agreement with this estimate is achieved for $\gamma_T = 6\text{–}8 \times 10^{-4}$ m s^{-1} (Figure 4a). For Helheim glacier, the range of observational melt rate estimates corresponds to simulations with γ_T varied over one order of magnitude. For Store glacier, $\gamma_T \sim 9 \times 10^{-4}$ m s^{-1} produces the observed melt rate. In summary, the application to realistic glacier settings confirms that $\gamma_T^* \sim 10^{-3} \pm 10^{-4}$ m s^{-1} can yield melt rates consistent with observational estimates.

In all three cases considered, the simulated relative contribution of melting within the subglacial discharge plume to the terminus averaged melt (gray lines in Figure 4) is small, less than 20% for LeConte and Store glacier, and below 40% for Helheim. Although the largest melt rates are found within the subglacial discharge plumes, they occupy a relatively small area of the glacier front. As a result, background melt (i.e., weaker submarine melting integrated over the remainder of the front) dominates terminus-wide submarine melt. This finding contrasts previous work (e.g., Beckmann et al., 2018; Cowton et al., 2015), but was already suspected by Chauché (2016, chapter 4), who reported submarine melting to persist after subglacial discharge decayed in winter. This apparent dominance of background melting underlines the importance of constraining the constant thermal transfer velocity at low ambient velocities, γ_T^* (see Section 4.1, Equation 11). We propose that the exact constraint of Γ_T and C_d is of secondary importance, influencing the melt rate only *within* subglacial discharge plumes (see Section 4.2, Equation 11).

The simplification of not simulating individual meltwater plumes (difference black and blue lines, Figure 4) overestimates terminus-integrated melt rates by 14% (LeConte), 17% (Helheim) and 23% (Store), for $\gamma_T^* = 10^{-3}$ m s^{-1}, and has negligible effect on the relative melt rate contributions (gray lines, blue stars, Figure 4). For practical application of our scheme, this simplification can provide useful melt estimates without high computational cost.

5. Uncertainties

Under the assumption that the applied theoretical framework summarized in Section 2 is valid, the sensitivity of the derived optimal value of $\gamma_T^* \sim 10^{-3}$ m s^{-1} to the uncertainty in the input parameters is small. Consistent with previous studies, our results are insensitive to the initial subglacial discharge up to a threshold of 10^{-8} m^3 s^{-1} (Jackson et al., 2020), and to the exact value of the ice temperature T_i (Cowton et al., 2015). In addition, substituting the ratio of $\gamma_{T,S}$ used here (Equation 5) with the ratio proposed in Jenkins et al. (2010) results in a change in γ_T^* much smaller than the uncertainty of $O(10^{-4}$ m s$^{-1})$ arising from observational uncertainties in the meltwater plume properties to which we are fitting.

The most critical uncertainty is whether or not boundary layers controlled by convective instabilities, as outlined in Section 2, are applicable to the submarine melting processes at the front of the LeConte glacier observed by Jackson et al. (2020). Laboratory experiments suggest that submarine melting is controlled by convective instabilities up to a threshold velocity of $u_t = 0.03$–0.05 m s^{-1} (McConnochie & Kerr, 2017). This threshold value is close to the average simulated meltwater plume velocities of 0.07 m s^{-1} presented here (Figure 1c), but lower than the ambient current velocities of order 0.2 m s^{-1} observed at a distance of ∼100 m from the LeConte glacier front (Jackson et al., 2020; Motyka et al., 2003). A recent assessment of sloping ice shelves in Antarctica (Rosevear et al., 2021) indicates that even in environments with relatively high background velocities of 0.1 m s^{-1}, observed melt rates were better reproduced using a parameterization assuming a boundary region controlled by convective instabilities (McConnochie & Kerr, 2018) instead of shear instabilities (Jenkins et al., 2010). In Greenland, melt environments are characterized by vertical glacier fronts and warmer ambient water. We propose that convectively-dominated melt regimes are even more plausible in the presence of stronger buoyancy forcing and the absence of geometrical constraints. Observational evidence is currently insufficient to reject our hypothesis that convective instabilities govern the ice-ocean exchange at LeConte glacier, even in the presence of relatively high observed ambient velocities. Ultimately, the applicability of our theoretical framework to LeConte glacier depends on how the thickness of the mm-thin laminar sublayer at the ice-ocean interface is controlled, a question that cannot be conclusively answered at this time.

6. Summary and Conclusions

Our study was motivated by an urgent need for a physically plausible and observationally informed melt rate parameterization for use in ocean circulation models. Here, we propose a new parameterization for submarine melting at vertical glacier fronts, consistent across low and high ambient velocity regimes, and with coefficients constrained by recently published unique observations of meltwater intrusions. The proposed parameterization includes a novel functional form, allowing for a linear superposition of contributions from shear instabilities and convective instabilities at high ambient velocities, for example, within a subglacial discharge plume, and a velocity–independent formulation at low ambient velocities, motivated by physical theory. It incorporates only a single free parameter, the thermal transfer velocity γ_T^*, which is observationally-constrained. The optimization of γ_T^* presented here can be revisited as additional observations at vertical glacier fronts become available. The novel sampling methods deployed by Jackson et al. (2020) offer an important opportunity for constraining melt around Greenland and faithfully representing melt dynamics in climate models.

An evaluation against observational estimates of melt rates for three non-floating marine terminating glaciers indicates that the melt rate parameterization proposed in this study performs well on the scale of the entire glacier front. Compared to the commonly used parameterization by Jenkins et al. (2010), originally derived for floating glacier tongues, our parameterization provides a greatly improved fit to observational data. Another important result from this study is the suggested dominance of background submarine melting over melting within subglacial discharge plumes, on a terminus-averaged scale. Hence, total submarine melt rates can be well approximated based on glacier front geometry and ambient temperature and salinity profiles alone.

Our parameterization can readily be used in ocean circulation models that do not explicitly resolve heat transfer across the ice-ocean interface, but resolve fjord dynamics. Implementation in ocean models that do not resolve fjord dynamics will require development of a suitable parameterization of the circulation within the fjord, followed by the transformation of subglacial discharge and melt water, and subsequent export from the fjord (Muilwijk et al., 2022). The improved quantification of submarine melting in numerical models based on our parameterization will enable the scientific community to address pressing questions related to a changing climate around Greenlands coastal margins. By better constraining submarine melt at glacier termini, we can improve the quantification of ice loss from the Greenland Ice Sheet in response to changes in fjord stratification and dynamics, the relative importance of terminus melting and calving, and the effects of submarine melting on the glacier flow. On the ocean side, improved melt rates allow to better constrain the fresh water input into glacial fjords and its effect on stratification and circulation strength and patterns. On a larger scale, a better quantification of fresh water input into the adjacent shelf seas and oceans will enable us to study the effect of increased mass loss of the Greenland Ice Sheet on global circulation patterns.

Data Availability Statement

Observational data used in this study is available at Sutherland et al. (2019b) for the LeConte Bay, Straneo (2022) for Helheim glacier/Sermilik Fjord, and Rignot and Schulz (2022) for Store fjord. The plume model used in this study builds on code developed by Cowton et al. (2015) and is distributed from Tom Cowton through his publicly available github open-source site https://github.com/tcowton/iceplume and open-source MITgcm checkpoint 65m https://github.com/MITgcm/MITgcm/archive/checkpoint65m.zip. Our modifications made to the iceplume package are available at https://github.com/KikiSchulz/iceplume_mod.

Acknowledgments
This work was supported by NSF-AccelNet-2020387 (ATN, KS) and NSF-OCE-1924546 (HRP). The authors would like to thank Rebecca Jackson for her extensive advice and the inspiring discussions, and for providing the observational data for this study. The numerical implementation of the melt rate parameterization builds up on excellent code written and provided by Tom Cowton. The authors would also like to thank Fiammetta Straneo, James Holte, and Eric Rignot for providing the hydrographic profiles used in Section 4.3, and everyone involved in the data acquisition and processing. For Store glacier, data acquisition and processing was performed at the University of California Irvine under a contract with the National Aeronautics and Space Administration Cryosphere Science Programs. The authors are grateful for the clarification on glacier terminology kindly provided by Lorenz Meire. The authors thank Michael Wood and the three anonymous reviewers, whose comments and suggestions greatly helped to improve the manuscript.

References

Bakker, P., Schmittner, A., Lenaerts, J., Abe-Ouchi, A., Bi, D., van den Broeke, M., et al. (2016). Fate of the Atlantic meridional overturning circulation: Strong decline under continued warming and Greenland melting. *Geophysical Research Letters*, *43*(23), 12–252. https://doi.org/10.1002/2016GL070457

Beckmann, J., Perrette, M., & Ganopolski, A. (2018). Simple models for the simulation of submarine melt for a Greenland glacial system model. *The Cryosphere*, *12*(1), 301–323. https://doi.org/10.5194/tc-12-301-2018

Böning, C. W., Behrens, E., Biastoch, A., Getzlaff, K., & Bamber, J. L. (2016). Emerging impact of Greenland meltwater on deepwater formation in the North Atlantic Ocean. *Nature Geoscience*, *9*(7), 523–527. https://doi.org/10.1038/ngeo2740

Chauché, N. (2016). *Glacier-ocean interaction at Store glacier (west Greenland)* (Unpublished doctoral dissertation). Aberystwyth University.

Cowton, T. R., Slater, D. A., Sole, A. J., Goldberg, D. A., & Nienow, P. W. (2015). Modeling the impact of glacial runoff on fjord circulation and submarine melt rate using a new subgrid-scale parameterization for glacial plumes. *Journal of Geophysical Research: Oceans*, *120*(2), 796–812. https://doi.org/10.1002/2014JC010324

Cowton, T. R., Sole, A. J., Nienow, P. W., Slater, D. A., & Christoffersen, P. (2018). Linear response of east Greenland's tidewater glaciers to ocean/atmosphere warming. *Proceedings of the National Academy of Sciences*, *115*(31), 7907–7912. https://doi.org/10.1073/pnas.1801769115

Fahrner, D., Lea, J. M., Brough, S., Mair, D. W., & Abermann, J. (2021). Linear response of the Greenland ice sheet's tidewater glacier terminus positions to climate. *Journal of Glaciology*, *67*(262), 193–203. https://doi.org/10.1017/jog.2021.13

Frajka-Williams, E., Bamber, J. L., & Våge, K. (2016). Greenland melt and the Atlantic meridional overturning circulation. *Oceanography*, *29*(4), 22–33. https://doi.org/10.5670/oceanog.2016.96

Gade, H. G. (1979). Melting of ice in sea water: A primitive model with application to the Antarctic ice shelf and icebergs. *Journal of Physical Oceanography*, *9*(1), 189–198. https://doi.org/10.1175/1520-0485(1979)009<0189:moiisw>2.0.co;2

Hellmer, H. H., & Olbers, D. J. (1989). A two-dimensional model for the thermohaline circulation under an ice shelf. *Antarctic Science*, *1*(4), 325–336. https://doi.org/10.1017/S0954102089000490

Hewitt, I. J. (2020). Subglacial plumes. *Annual Review of Fluid Mechanics*, *52*(1), 145–169. https://doi.org/10.1146/annurev-fluid-010719-060252

Holland, D. M., & Jenkins, A. (1999). Modeling thermodynamic ice–ocean interactions at the base of an ice shelf. *Journal of Physical Oceanography*, *29*(8), 1787–1800. https://doi.org/10.1175/1520-0485(1999)029<1787:mtioia>2.0.co;2

Huhn, O., Rhein, M., Kanzow, T., Schaffer, J., & Sültenfuß, J. (2021). Submarine meltwater from Nioghalvfjerdsbræ (79 North Glacier), Northeast Greenland. *Journal of Geophysical Research: Oceans*, *126*(7), e2021JC017224. https://doi.org/10.1029/2021JC017224

Jackson, R. H., Nash, J., Kienholz, C., Sutherland, D., Amundson, J., Motyka, R., et al. (2020). Meltwater intrusions reveal mechanisms for rapid submarine melt at a tidewater glacier. *Geophysical Research Letters*, *47*(2), e2019GL085335. https://doi.org/10.1029/2019GL085335

Jackson, R. H., Shroyer, E. L., Nash, J. D., Sutherland, D. A., Carroll, D., Fried, M. J., et al. (2017). Near-glacier surveying of a subglacial discharge plume: Implications for plume parameterizations. *Geophysical Research Letters*, *44*(13), 6886–6894. https://doi.org/10.1002/2017GL073602

Jackson, R. H., & Straneo, F. (2016). Heat, salt, and freshwater budgets for a glacial fjord in Greenland. *Journal of Physical Oceanography*, *46*(9), 2735–2768. https://doi.org/10.1175/JPO-D-15-0134.1

Jenkins, A. (1991). A one-dimensional model of ice shelf-ocean interaction. *Journal of Geophysical Research*, *96*(C11), 20671–20677. https://doi.org/10.1029/91JC01842

Jenkins, A. (2011). Convection-driven melting near the grounding lines of ice shelves and tidewater glaciers. *Journal of Physical Oceanography*, *41*(12), 2279–2294. https://doi.org/10.1175/JPO-D-11-03.1

Jenkins, A., Nicholls, K. W., & Corr, H. F. (2010). Observation and parameterization of ablation at the base of Ronne ice shelf, Antarctica. *Journal of Physical Oceanography*, *40*(10), 2298–2312. https://doi.org/10.1175/2010JPO4317.1

Josberger, E. G., & Neshyba, S. (1980). Iceberg melt-driven convection inferred from field measurements of temperature. *Annals of Glaciology*, *1*, 113–117. https://doi.org/10.3189/S0260305500017080

Kerr, R. C., & McConnochie, C. D. (2015). Dissolution of a vertical solid surface by turbulent compositional convection. *Journal of Fluid Mechanics*, *765*, 211–228. https://doi.org/10.1017/jfm.2014.722

King, M. D., Howat, I. M., Candela, S. G., Noh, M. J., Jeong, S., Noël, B. P., et al. (2020). Dynamic ice loss from the Greenland Ice Sheet driven by sustained glacier retreat. *Communications Earth & Environment*, *1*(1), 1–7. https://doi.org/10.1038/s43247-020-0001-2

Le Bras, I. A.-A., Straneo, F., Holte, J., & Holliday, N. P. (2018). Seasonality of freshwater in the east Greenland current system from 2014 to 2016. *Journal of Geophysical Research: Oceans*, *123*(12), 8828–8848. https://doi.org/10.1029/2018JC014511

Malyarenko, A., Wells, A. J., Langhorne, P. J., Robinson, N. J., Williams, M. J., & Nicholls, K. W. (2020). A synthesis of thermodynamic ablation at ice-ocean interfaces from theory, observations and models. *Ocean Modelling*, *154*, 101692. https://doi.org/10.1016/j.ocemod.2020.101692

McConnochie, C. D., & Kerr, R. C. (2017). Testing a common ice-ocean parameterization with laboratory experiments. *Journal of Geophysical Research: Oceans*, *122*(7), 5905–5915. https://doi.org/10.1002/2017JC012918

McConnochie, C. D., & Kerr, R. C. (2018). Dissolution of a sloping solid surface by turbulent compositional convection. *Journal of Fluid Mechanics*, *846*, 563–577. https://doi.org/10.1017/jfm.2018.282

McPhee, M. G., Maykut, G. A., & Morison, J. H. (1987). Dynamics and thermodynamics of the ice/upper ocean system in the marginal ice zone of the Greenland sea. *Journal of Geophysical Research*, *92*(C7), 7017–7031. https://doi.org/10.1029/JC092iC07p07017

Motyka, R. J., Hunter, L., Echelmeyer, K. A., & Connor, C. (2003). Submarine melting at the terminus of a temperate tidewater glacier, LeConte Glacier, Alaska, USA. *Annals of Glaciology*, *36*, 57–65. https://doi.org/10.3189/172756403781816374

Mouginot, J., Rignot, E., Bjørk, A. A., Van den Broeke, M., Millan, R., Morlighem, M., et al. (2019). Forty-six years of Greenland Ice Sheet mass balance from 1972 to 2018. *Proceedings of the National Academy of Sciences*, *116*(19), 9239–9244. https://doi.org/10.1073/pnas.1904242116

Muilwijk, M., Straneo, F., Slater, D. A., Smedsrud, L. H., Holte, J., Wood, M., et al. (2022). Export of ice sheet meltwater from Upernavik fjord, west Greenland. *Journal of Physical Oceanography*, *52*(3), 363–382. https://doi.org/10.1175/JPO-D-21-0084.1

Rignot, E., & Schulz, K. (2022). Vertical profiles of ocean temperature and salinity near Store glacier, West Greenland, August 2010 [dataset]. Arctic Data Center. https://doi.org/10.18739/A20R9M52T

Rosevear, M. G., Galton-Fenzi, B. K., & Stevens, C. (2021). Evaluation of basal melting parameterisations using in situ ocean and melting observations from the Amery Ice Shelf, East Antarctica. *Ocean Science Discussions*, *2021*, 1–31. https://doi.org/10.5194/os-2021-111

Scheduikat, M., & Olbers, D. J. (1990). A one-dimensional mixed layer model beneath the Ross Ice Shelf with tidally induced vertical mixing. *Antarctic Science*, *2*(1), 29–42. https://doi.org/10.1017/S0954102090000049

Sciascia, R., Straneo, F., Cenedese, C., & Heimbach, P. (2013). Seasonal variability of submarine melt rate and circulation in an East Greenland fjord. *Journal of Geophysical Research: Oceans*, *118*(5), 2492–2506. https://doi.org/10.1002/jgrc.20142

Slater, D. A., Nienow, P. W., Cowton, T. R., Goldberg, D. N., & Sole, A. J. (2015). Effect of near-terminus subglacial hydrology on tidewater glacier submarine melt rates. *Geophysical Research Letters*, *42*(8), 2861–2868. https://doi.org/10.1002/2014GL062494

Straneo, F. (2022). Profiles of temperature, salinity, and turbidity from Sermilik fjord during August 2009 [dataset]. Arctic Data Center. https://doi.org/10.18739/A2R785Q4V

Straneo, F., & Cenedese, C. (2015). The dynamics of Greenland's glacial fjords and their role in climate. *Annual Review of Marine Science*, *7*(1), 89–112. https://doi.org/10.1146/annurev-marine-010213-135133

Straneo, F., Curry, R. G., Sutherland, D. A., Hamilton, G. S., Cenedese, C., Våge, K., & Stearns, L. A. (2011). Impact of fjord dynamics and glacial runoff on the circulation near Helheim Glacier. *Nature Geoscience*, *4*(5), 322–327. https://doi.org/10.1038/ngeo1109

Straneo, F., & Heimbach, P. (2013). North Atlantic warming and the retreat of Greenland's outlet glaciers. *Nature*, *504*(7478), 36–43. https://doi.org/10.1038/nature12854

Sutherland, D. A., Jackson, R. H., Kienholz, C., Amundson, J. M., Dryer, W., Duncan, D., et al. (2019a). Direct observations of submarine melt and subsurface geometry at a tidewater glacier. *Science*, *365*(6451), 369–374. https://doi.org/10.1126/science.aax3528

Sutherland, D. A., Jackson, R. H., Kienholz, C., Amundson, J. M., Dryer, W. P., Duncan, D., et al. (2019b). Water temperature, salinity, currents, and others collected by CTD and ADCP from MV Steller and MV pelican in LeConte Bay, Alaska from 2016-08-09 to 2018-09-18 (NCEI accession 0189574) [dataset]. NOAA National Centers for Environmental Information. Retrieved from https://www.ncei.noaa.gov/archive/accession/0189574

Sutherland, D. A., & Straneo, F. (2012). Estimating ocean heat transports and submarine melt rates in Sermilik Fjord, Greenland, using lowered acoustic Doppler current profiler (LADCP) velocity profiles. *Annals of Glaciology*, *53*(60), 50–58. https://doi.org/10.3189/2012AoG60A050

Thornalley, D. J., Oppo, D. W., Ortega, P., Robson, J. I., Brierley, C. M., Davis, R., et al. (2018). Anomalously weak Labrador Sea convection and Atlantic overturning during the past 150 years. *Nature*, *556*(7700), 227–230. https://doi.org/10.1038/s41586-018-0007-4

Wells, A. J., & Worster, M. G. (2008). A geophysical-scale model of vertical natural convection boundary layers. *Journal of Fluid Mechanics*, *609*, 111–137. https://doi.org/10.1017/S0022112008002346

Wood, M., Rignot, E., Fenty, I., An, L., Bjørk, A., van den Broeke, M., et al. (2021). Ocean forcing drives glacier retreat in Greenland. *Science Advances*, *7*(1), eaba7282. https://doi.org/10.1126/sciadv.aba7282

Xu, Y., Rignot, E., Fenty, I., Menemenlis, D., & Flexas, M. M. (2013). Subaqueous melting of Store Glacier, west Greenland from three-dimensional, high-resolution numerical modeling and ocean observations. *Geophysical Research Letters*, *40*(17), 4648–4653. https://doi.org/10.1002/grl.50825

Yang, Q., Dixon, T. H., Myers, P. G., Bonin, J., Chambers, D., Van Den Broeke, M., et al. (2016). Recent increases in Arctic freshwater flux affects Labrador Sea convection and Atlantic overturning circulation. *Nature Communications*, *7*(1), 1–8. https://doi.org/10.1038/ncomms10525